Oscillations and Sparsening of Odor Representations in the Mushroom Body

Javier Perez-Orive,* Ofer Mazor,* Glenn C. Turner, Stijn Cassenaer, Rachel I. Wilson, Gilles Laurent†

In the insect olfactory system, oscillatory synchronization is functionally relevant and reflects the coherent activation of dynamic neural assemblies. We examined the role of such oscillatory synchronization in information transfer between networks in this system. The antennal lobe is the obligatory relay for olfactory afferent signals and generates oscillatory output. The mushroom body is responsible for formation and retrieval of olfactory and other memories. The format of odor representations differs significantly across these structures. Whereas representations are dense, dynamic, and seemingly redundant in the antennal lobe, they are sparse and carried by more selective neurons in the mushroom body. This transformation relies on a combination of oscillatory dynamics and intrinsic and circuit properties that act together to selectively filter and synthesize the output from the antennal lobe. These results provide direct support for the functional relevance of correlation codes and shed some light on the role of oscillatory synchronization in sensory networks.

Electroencephalogram and local field potential (LFP) oscillations generally indicate periodic coherent synchronization of neuronal assemblies (*1–6*). Although the occurrence of macroscopic oscillations has now been correlated with various sensory, behavioral, or cognitive states in mammals (*7–12*), the functional significance of such observations is debated (*13*, *14*). Many hypotheses based on temporal correlations have been proposed (*14–17*); among others, one proposes that cortical neurons might act as coincidence detectors instead of integrators and thus select for correlated input (*18*, *19*). Most hypotheses, however, remain tentative for lack of a direct experimental test. The olfactory nervous system, in which molecular design (*20–23*), circuit architecture (*23*), and oscillatory dynamics (*1*, *2*, *24*, *25*) appear common across phyla, offers a rare opportunity to study some of these coding issues.

Olfactory Circuits

The insect antennal lobe (AL) is the analog of the vertebrate olfactory bulb. In locusts, each AL receives input from about 90,000 olfactory receptor neurons and contains about 1130 densely interconnected neurons [300 local inhibitory neurons and 830 excitatory, multiglomerular projection neurons (PNs)] (*24*, *26–29*). Each AL sends distributed projections to the ipsilateral mushroom body (MB), a memory area (*30–33*) (fig. S1). PNs are the only channel for olfactory input to the MB. Conversely, there is no evidence for feedback from the MB to the AL. Each locust MB contains about 50,000 small neurons [Kenyon cells (KCs)] (*24*, *34*), whose spiny dendrites receive direct input from PNs (*24*). In locusts, each PN contacts about 600 KCs (about 30 synaptic varicosities per PN axon times about 20 distinct synaptic contacts with different KC profiles per varicosity) (*35*). Each KC receives contacts from many PNs, as indicated by incremental electrical stimulation of PNs. The total number of outputs made by all PNs onto KCs must equal the total number of PN inputs received by all KCs; hence, if 830 PNs project to 50,000 KCs with 1:600 divergence, the average PN-to-KC convergence is on the order of 10. Although it remains unknown, these ratios probably vary little more than a few fold across the PN/KC populations. The dendritic tree of a typical KC contains 100 to 200 spines (*24*). Many of these inputs must thus originate outside the AL.

Odor-evoked PN responses exhibit globally coherent 20- to 30-Hz oscillations and stimulus- and PN-specific slow modulation of firing rate, both shaped in great part by local neuron–mediated inhibition (*26–29*, *36*). Hence, during a stimulus, the AL output consists of barrages of spikes from an evolving PN assembly. Although individual PN spike timing during one oscillation cycle can be phase-locked, this locking does not occur for all PNs active during that cycle. At what time(s) a PN locks to others depends on both the odor and the PN. To understand the decoding of PN output by KCs, we examine the firing behavior of both populations at rest and in response to odors.

Division of Biology, 139-74, California Institute of Technology, Pasadena, CA 91125, USA.

*These authors contributed equally to this work.
†To whom correspondence should be addressed. E-mail: laurentg@caltech.edu.

Resting Activity

We measured baseline activity profiles of PNs and KCs over stretches of uninterrupted recording several minutes long in naïve animals, with multiple tetrode recordings (*37*) (fig. S2). At rest, the PN population fired at a mean rate of 3.87 ± 2.23 spikes per s per PN (range, 0.49 to 10.4; n = 35 PNs). Baseline firing was >100 times lower in KCs (median, 0.025 spike per s; interquartile range, 0.088 spike per s; n = 23 KCs) (fig. S3). Hence, despite a constant excitatory drive from PNs, KCs at rest remained remarkably inactive.

Response Selectivity

We challenged PNs and KCs in awake animals with a panel of odors (typically 17; range, 5 to 24; 5 to 25 trials per odor; 1-s pulses; 20 to 30 s between trials) (*37*). Experimental conditions were identical for PN and KC recordings.

Spiking response probability. The probability of observing a stimulus-evoked change in firing behavior was different across the two populations (Fig. 1). Most PNs exhibited a reliable change in firing behavior within the first few seconds after stimulus onset. They showed complex temporal patterning (with increases and decreases in instantaneous firing rate) that often greatly outlasted the stimulus itself (Fig. 1A). Many of these responses were inhibitory, and many of these inhibitory periods were followed by a period of increased firing, up to 5 s after stimulus offset. We analyzed excitatory response probabilities across PNs (and KCs) quantitatively by a variety of methods and analysis windows. We show here the results obtained with method A (*37*). Results obtained with the other methods are nearly identical (figs. S4 and S5). The distribution of response probabilities for PNs was broad (Fig. 2A), with a mean over all cells of 0.64 (median, 0.74; interquartile range, 0.57; n = 58 PNs, 1140 PN-odor pairs). KC responses to these same odors were extremely rare: over all KCs (n = 74 KCs, 1101 KC-odor pairs), 58% failed to show any detectable response to any of the odors presented (Fig. 2A). The distribution of response probabilities was heavily skewed toward low values (Fig. 2A), even when only those KCs that produced at least one response were considered. The mean response probability, after averaging all the individual response probabilities of the KCs was 0.11 (Fig. 2A) (median, 0.00; interquartile range, 0.12). Figure 1B shows three typical responsive KCs. Among all recorded KCs, only two responded to all odors presented (8 and 10 odors, respectively). To avoid possible sampling bias, we made recordings from all regions and depths of the KC soma layers. We found responsive and unresponsive KCs everywhere, which is consistent with the anatomy of PN axonal projections in the MB (*24*). Similarly, no selection bias toward strong responses existed, for the great majority of them were extremely brief and were rarely detected during the recording. Selective and

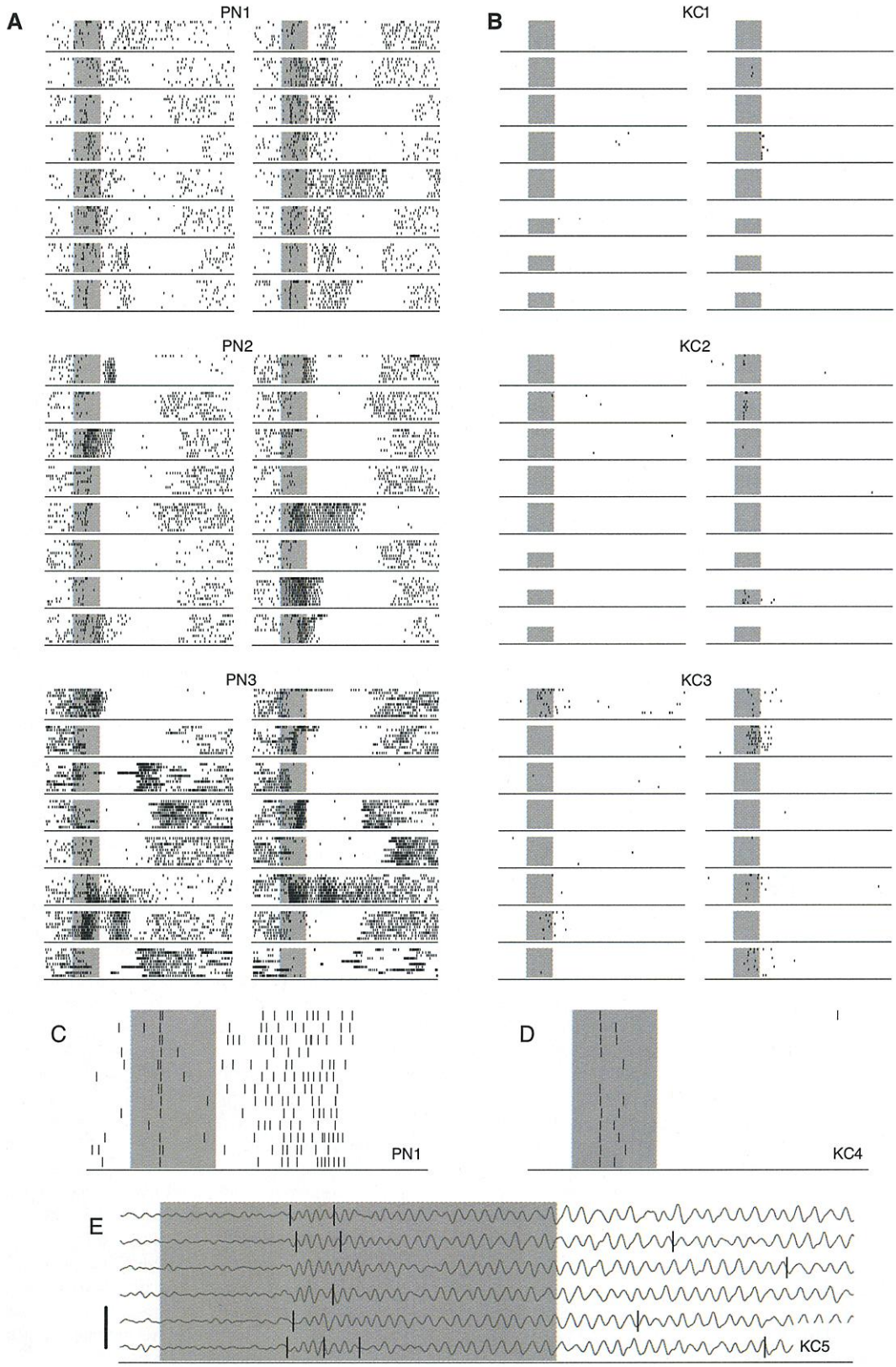

Fig. 1. In vivo tetrode recordings of odor responses in PNs (**A** and **C**) and KCs (**B**, **D**, and **E**). Shaded area, odor puff (1 s). (A) Responses of three simultaneously recorded PNs (PN1 to PN3) to 16 different odors (first 10 trials with each stimulus displayed, top to bottom). Odors from top, left column: hpo, don, che, hx3, unn, min, oca, pnn; right column: chx, oco, nnn, thx, 2hp, nna, 3hp, hxo (*37*). Abbreviations are as follows: 1-hexen-3-ol (hx3), *trans*-2-hexen-1-ol (thx), *cis*-3-hexen-1-ol (chx), 1-hexanol (hxo), 1-heptanol (hpo), 1-octanol (oco), hexanal (hxa), heptanal (hpa), octanal (oca), nonanal (nna), 3,7-dimethyl-2,6-octadiene-nitrile (don), 3-pentanone (pnn), 2-heptanone (2hp), 3-heptanone (3hp), 5-nonanone (nnn), 6-undecanone (unn), cherry (che), mint (min), geraniol (ger), vanilla (van), citral (cit), apple (app), strawberry (str), amylacetate (ama), benzaldehyde (bnh), methyl salicylate (mts), eugenol (eug), L-carvone (lca), D-carvone (dca), dihydro-myrcenol (dhm). (B) Responses of 3 KCs to the same 16 odors. Conditions are the same as in (A) with the following exceptions: for six of the odors, KC1 and KC2 have only five trials; in KC2, the seventh odor in the right column is hxa. (C) Expanded view of PN1 rasters in response to hxo (trials 3 to 15). Note alignment of spikes. (D) Response of a fourth KC to hx3 (trials 3 to 15). Note low baseline activity and alignment of first spike in the response across trials. (E) Response of a fifth KC with superimposed LFP, recorded in the MB (10- to 55-Hz bandpass). Note phase-locking of KC spikes. LFP = 400 μV.

promiscuous KCs could occur simultaneously on the same tetrode, which indicates that differences in tuning width were not caused by global modulation of excitability over time.

Response intensity. Response patterns and intensities differed in PNs and KCs. Whereas PN responses often lasted several seconds (Fig. 1A), KC responses were brief and lacked the slow temporal patterning typical of PNs (Fig. 1B). Using responsive cell-odor pairs, we counted action potentials produced by PNs and KCs over the 3-s window after stimulus onset. The distribution of PN spike counts over that period was broad, with a mean of 19.53 ± 10.67 spikes. KCs responded with 2.32 ± 2.68 spikes (Fig. 2A) (*38*). We found a negative correlation between KC spike count and response selectivity (Spearman-ranked

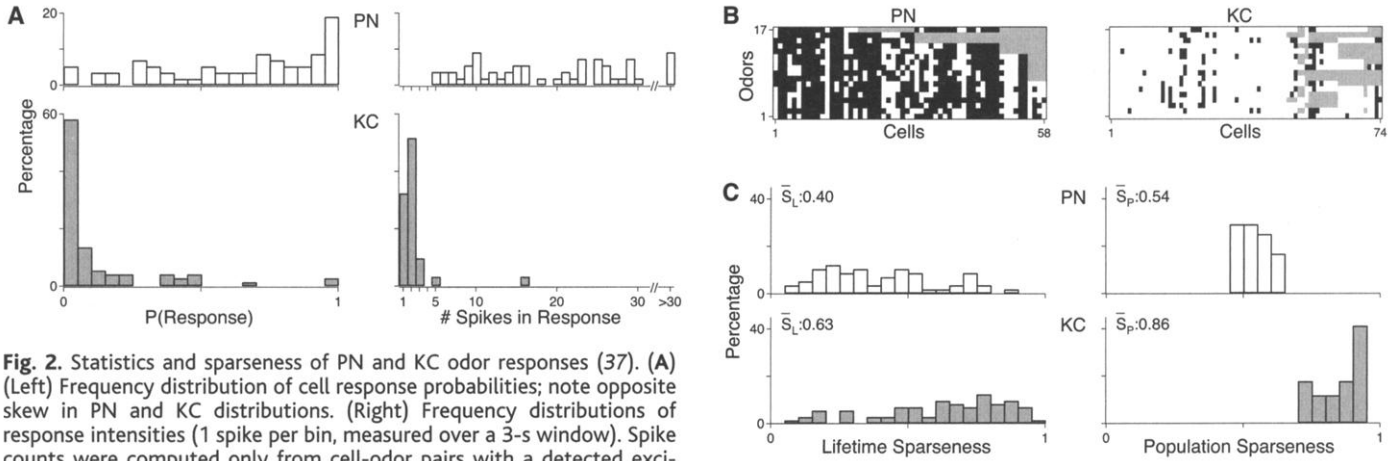

Fig. 2. Statistics and sparseness of PN and KC odor responses (*37*). (**A**) (Left) Frequency distribution of cell response probabilities; note opposite skew in PN and KC distributions. (Right) Frequency distributions of response intensities (1 spike per bin, measured over a 3-s window). Spike counts were computed only from cell-odor pairs with a detected excitatory response. (**B**) Excitatory responses (filled squares) of individual PNs and KCs (columns) (n = 58 PNs, 74 KCs) to 17 different odors (rows: hx3, thx, chx, hxo, hpo, oco, nna, nnn, don, pnn, 2hp, 3hp, oca, unn, che, min, hxa) (*37*). Abbreviations are as in Fig. 1. Open squares denote inhibition (PNs only) or absence of a response. Gray squares indicate not tested. (**C**) Distributions of lifetime (left) and population (right) sparseness, computed across all cells and all tested odors. S_L and S_P are significantly different across PNs and KCs ($P < 0.001$, t test for S_P, z statistic for S_L).

correlation coefficient, −0.567, $P < 0.05$).

Temporal precision. PN spike probability and precision is PN, odor, and time specific (*26–29*, *36*). Time-locked PN spikes were easily detected when they occurred in isolation (for example, Fig. 1C), but they were also found within sustained responses, which is consistent with previous intracellular results. In KCs, individual responses typically contained about two spikes (Fig. 2A), at least one of which could be precisely locked to stimulus onset with a fixed delay. Stimulus-locked spikes were often the first ones in the response of the KCs but could occur at any cycle. The first spike in the response of KC4 (Fig. 1D), for example, had a jitter of only ±4 ms relative to stimulus onset. Stimulus-locked spikes with such small jitter, however, were not commonly observed. Another measure of precision more relevant to this system is the timing of each action potential relative to its LFP oscillation cycle (phase) (Fig. 1E). The mean phase of KC spikes was 83° ± 77° (n = 18 KCs; 0° is oscillation peak). Mean spike phase was the same in the most- and in the least-specific KCs (90° ± 67° versus 86° ± 81°; n = 5 cells each). The spikes within a doublet (or triplet) were typically separated by one to a few oscillation cycles (Fig. 1E). This indicates that appropriate PN drive to individual KCs lasted several oscillation cycles and that, when a KC spike was fired, it occurred preferentially at the same phase of its oscillation cycle.

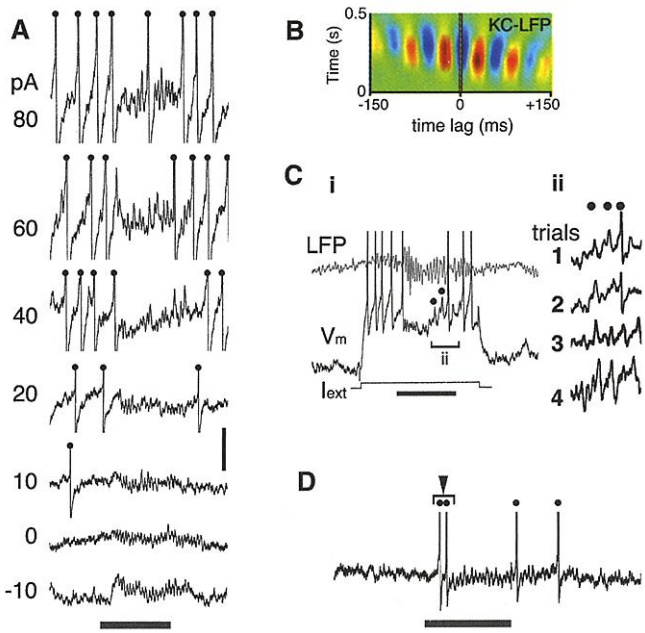

Fig. 3. In vivo sharp-electrode intracellular records from different KCs. All action potentials are clipped. (**A**) Responses obtained while resting voltage was set by holding currents between −10 and +80 pA. Horizontal bar, odor (cherry) delivery (800 ms). This KC never produced any action potential in response to this odor at resting potential. Note oscillating membrane potential at rest (0 pA), interruption of direct current-evoked firing by odor delivery (+20- to 80-pA traces), and amplification of many discrete depolarizing potentials at most depolarized holding potentials. (**B**) Sliding cross-correlation of KC V_m and simultaneous LFP during hexanol odor puff [different KC from that in (A)]. Red, maxima; blue, minima. y axis: time, 0.5 s. Note locking of signals during odor puff. (**C**) Third KC recording, showing interruption of current-evoked firing by cherry odor response and prominent, late EPSPs (·); 800-ms odor delivery (i). Repeated trials (1 to 4) show precise reoccurrence of these EPSPs during the same epoch of the response; time calibration, 500 ms (ii). (**D**) Fourth KC and its spiking response to cherry odor at cycles 1 and 3; 800-ms odor pulse. Vertical calibrations: KC, 10 mV (A and D), 8 mV (Ci), 6 mV (Cii); LFP, 300 μV, 1- to 40-Hz bandpass (C).

Sparseness of Odor Representations Across PNs and KCs

Figure 2B compresses the responses of 58 PNs and 74 KCs to the same 17 odors and illustrates the contrast between the two population representations (*39*). A simple estimate of population sparseness (S_P) is the proportion of cells unresponsive to each stimulus averaged over all stimuli. It thus represents the sparseness of the representation of each odor across the population, averaged over all odors, but ignores the strength of each response. S_P was 0.90 in KCs and 0.33 in PNs. S_P can also be calculated without relying on how a response is defined by using firing rate distributions for each tested stimulus, whether we detected a response or not (*37*, *40*). Applied to PNs and KCs, this measure of S_P was always greater in KCs (Fig. 2C). Lastly, sparseness can be calculated for each cell across all the stimuli it has experienced. This measure, called lifetime sparseness, S_L, approximates the mean tuning width of each neuron averaged over all neurons. Again, S_L was significantly higher in KCs than in PNs ($P < 0.001$, t test) (Fig. 2C). S_L and S_P were also calculated by using the other response analysis windows or by using only the odor-responsive cells. By all measures, odor representations were always significantly sparser across KCs than across PNs (figs. S4 and S5).

Mechanisms Underlying Sparsening

Subthreshold KC activity during odor stimulation. Sharp electrode recordings (*37*) from

KCs (n = 29) revealed odor-evoked, subthreshold activity made up of periodic synaptic potentials (Fig. 3A). These were locked to the LFP (Fig. 3B) and superimposed on a noisy and irregular synaptic background away from the firing threshold. Appropriate odor-KC combinations revealed reliable and time-specific excitatory postsynaptic potentials (EPSPs) and/or action potentials. The response of the KC in Fig. 3C, for example, contained a train of prominent EPSPs late within the stimulus. One of these EPSPs led to an action potential in half of all trials with that odor. A different KC responded to the same odor with at least two reliable action potentials, at cycles 1 and 3 of the response, whether the neuron was at rest (Fig. 3D) or was held depolarized by current injection. In all tested KCs, the existence, timing, and reliability of these firing events were odor specific. We noted that a large component of the odor-evoked activity in KCs was inhibitory: If the KC was held depolarized by current injection, periodic hyperpolarizing potentials could be seen during a response; if the KC was held above firing threshold, odor-evoked inhibition interrupted this tonic firing (Fig. 3, A and C). Thus, odor stimulation also causes synaptic inhibition of KCs. Finally, the amplitude of odor-evoked EPSPs paradoxically increased when the KC was held depolarized (Fig. 3A), which suggests active membrane properties. We examined the possibility that synaptic inhibition and KC active conductances work together to make KCs coincidence detectors of PN input.

Source of masked odor-evoked inhibition. Because direct effects of PNs are excitatory and because locust PNs do not contain γ-aminobutyric acid (GABA) (*35*), the source of odor-evoked KC inhibition should be downstream of PNs. In addition to sending collaterals into the MB, PN axons terminate in the lateral horn (*41*). We identified among their targets there a cluster of about 60 GABA-immunoreactive neurons [lateral horn interneurons (LHIs)], with direct axonal projections to the MB (*37*) (Fig. 4A; Movie S1). Intracellular staining of individual LHIs showed profuse axonal collaterals, overlapping with KC dendrites (Fig. 4B). KC dendrites receive GABAergic input (*35*). LHIs thus are well suited to be a source of the odor-evoked inhibitory inputs.

LHI responses to odors. LHIs responded vigorously and reliably to odors (Fig. 4, C and D). LHI membrane potential oscillated in phase with the LFP (Fig. 4E), and, when sufficiently excited, LHIs fired one or a short burst of action potentials at each oscillation cycle (Fig. 4C). In each cycle, LHI mean firing time lagged 173° behind that of PNs (Fig. 4F). LHI firing phase was independent of odor identity. Synaptic drive to KCs thus likely consists of EPSPs from PNs alternating with inhibitory postsynaptic potentials (IPSPs) from LHIs, occurring preferentially in opposite halves of each oscillation cycle (Fig. 4, F and G). PN and LHI inputs to KCs differ in one important respect: Because each KC on average receives inputs from a very small fraction of the PNs and because the firing probability and phase-locking of each PN typically evolves during a response, the probability that many of the PNs presynaptic to a given KC fire together within the same half of one oscillation cycle is low. By contrast, individual LHIs showed sustained responses to all odors presented (Fig. 4D), consistent with the fact that 830 PNs converge onto only about 60 LHIs. Because LHI axons diverge profusely in the MB (Fig. 4B), individual KCs should receive periodic input composed of consistent IPSPs, alternating with EPSPs whose total strength strongly depends on the stimulus.

Sharpening of KC responses to direct PN stimulation. We next tested more directly whether both synaptic inhibition and intrinsic active conductances assist coincidence detection in KCs. To study single EPSP-IPSP cycles in isolation, we used direct electrical stimulation of PNs instead of odors. Evoked postsynaptic potentials in KCs dramatically changed shape and duration when we varied stimulus strength (Fig. 5A). At high stimulus intensities, a sharp "spikelet" rode atop the depolarizing potential, which suggests active conductances (Fig. 5A, top trace). This spikelet was not an artifact of unusually strong stimuli: When we used a weak stimulus to elicit a smaller EPSP and adjusted holding current so that the KC was near firing threshold, spikelets could also be observed (Fig. 5B) (*37*, *42*, *43*). Next, we tested the idea that GABAergic feed-forward inhibition also shapes PN-evoked PSPs. At voltages below spikelet threshold, EPSP shape remained strongly voltage dependent (Fig. 5C). Local injection of picrotoxin (PCT), a $GABA_A$-like chloride channel blocker, into the MB calyx (*37*) broadened the

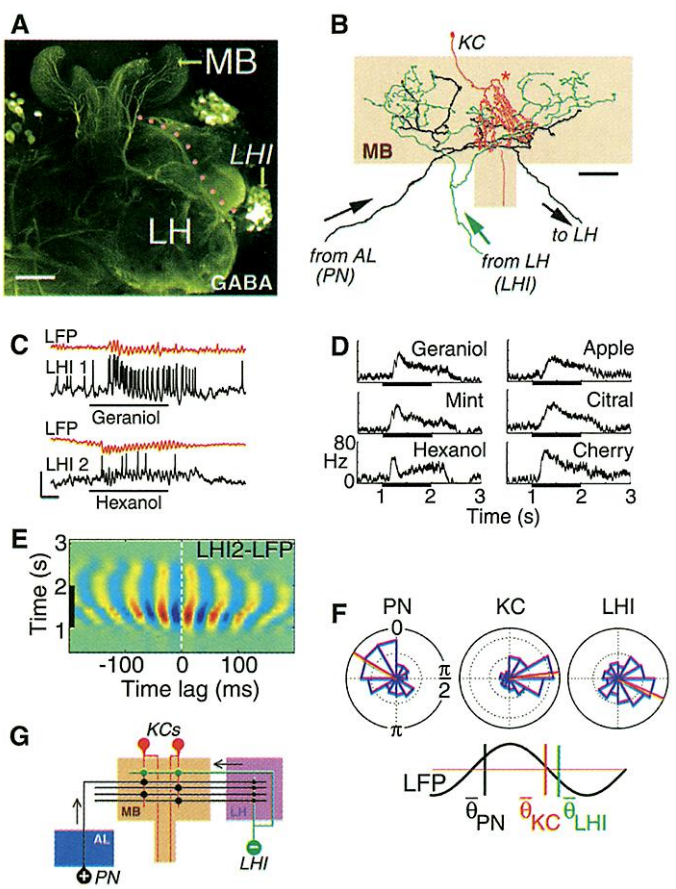

Fig. 4. Feed-forward inhibition of KCs by LHIs. (**A**) Immunolabeling by antibody to GABA (*37*). Cluster of about 60 reactive somata (LHI) and tract of LHI axons running to the MB (stipples) are shown. The terminals of one of these axons in the MB are shown in (B). Bar, 100 μm. (**B**) PN axon (black) projects to the MB calyx (orange) and to the lateral horn (LH) (*41*). LHI axon (green) projects to the calyx (this study). PN and LHI axons terminate on KC dendrites (red). Neurons were stained by iontophoresis of cobalt hexamine (KC, PN) or neurobiotin (LHI) in separate preparations and were drawn with a camera lucida. Note varicosities in LHI and PN axon collaterals. Asterisk, KC axon. Bar, 50 μm. (**C**) Representative odor-evoked responses of two LHIs and simultaneously recorded LFPs (5- to 40-Hz bandpass). Note membrane potential oscillations, locked to the LFP. Identity and delivery (1 s long) of stimulus indicated by black bar. LHI, 20 mV; LFP, 400 μV; 200 ms. (**D**) Instantaneous firing rate of LHI1 [in (C)] in response to various odors. Lower edge of profile shows mean instantaneous rate averaged across trials; profile thickness, SD. All LHIs responded to all odors tested, with response profiles that varied little across different odors. (**E**) Sliding cross-correlation between LFP and LHI2 traces (spikes clipped). Red, maxima; blue, minima. Strong locking is present throughout the response (odor delivery, vertical bar). Lower edge of correlation stripes just precedes stimulus onset due to width of the correlation window (200 ms). (**F**) Phase relationships between PN, KC, and LHI action potentials, and LFP. (Upper) Polar plots. LFP cycle maxima defined as 0 rad, minima as π rad (PNs: 3 cell-odor pairs, 388 spikes; LHIs: 17 cell-odor pairs, 2632 spikes; KCs: 18 cells, 862 spikes). Mean phases are shown in red. Gridlines are scaled in intervals of 0.10 (probability per bin). (Lower) Schematic diagram showing LFP and mean firing phases θ. (**G**) Circuit diagram.

EPSP and decreased the voltage dependence of EPSP shape (Fig. 5C). This indicates that the LHI-mediated IPSP normally contributes to the shape and duration of PN-evoked EPSPs. Blocking inhibition in the calyx increased the scatter of KC spike times after PN stimulation (Fig. 5D). LHI-mediated IPSPs thus contribute to shortening the epoch during which a KC remains depolarized after each volley of PN excitation; it could also explain why KC action potentials are so precisely phase-locked during responses to odors (Fig. 4F). Hence, the tendency of each KC to convert its excitatory input from PNs into an action potential can be facilitated in the early phase of the compound EPSP by voltage-dependent depolarizing nonlinearities, and it can be antagonized shortly thereafter by feed-forward inhibition. The remaining voltage dependence of the EPSP after PCT injection (Fig. 5C) suggests the existence of an active repolarizing conductance. Thus, both active and synaptic properties probably contribute to making KCs prefer coincident input on a cycle-by-cycle basis.

Influence of Feed-Forward Inhibition on KC Responses to Odors

If feed-forward inhibition competes with and resets the periodic excitation of KCs by PNs, antagonizing LHI-mediated inhibition should decrease KC specificity to odors. We tested KCs recorded in vivo with tetrodes with up to 17 odors (10 trials per odor) and retested them immediately after PCT injection into the MB (Fig. 6). PCT caused no significant change in the KC baseline-firing rate (median, 0.018 spike per s after PCT versus 0.005 before; $n = 12$ KCs, $P = 0.19$, nonparametric sign test). PCT caused a broadening of KC tuning, characterized by greatly reduced odor selectivity (Fig. 6, A to C). Even in KCs that responded to none of the odors presented in controls, responses to these same odors appeared after PCT (Fig. 6, A to C). Individual KCs did not become responsive to all odors but rather to a larger subset of all tested odors. The mean population and lifetime sparseness calculated over this KC subset was significantly decreased after PCT (S_P = 0.70 to 0.41, $n = 11$ odors, $P < 0.001$, paired t test; S_L = 0.47 to 0.30, $n = 12$ KCs, $P < 0.05$, nonparametric Wilcoxon signed-rank test). Individual KC response intensity after PCT treatment was not significantly different from control (control, 1.96 ± 0.81 spikes; PCT treatment, 1.82 ± 0.47 spikes), but KC action potentials after PCT lost their locking to the LFP (*44*) (Fig. 6D; controls, Fig. 4F). This confirms earlier experiments (Fig. 5, C and D), which suggest that LHI-mediated IPSPs normally constrain KC integration and spike timing.

Discussion

In the AL, individual odors are represented by a large fraction of the 830 PNs: Baseline activity is high, sparseness is low, and individual PN responses are sustained. In the MB, the same odors activate a small proportion of neurons in a larger population (50,000 KCs): baseline activity is close to 0, sparseness is high, and individual KC responses are rare and typically contain only two action potentials. KC action potentials thus each carry much more information than those of PNs.

How does sparsening arise? We propose that KCs act as selective coincidence detectors on periodic PN input. Because individual KCs receive inputs from only a small fraction of PNs, because the patterned responses of individual PNs are staggered in time, and because EPSP summation by KCs occurs best within a fraction of each oscillation cycle, the conditions appropriate for bringing a KC to threshold are rarely met. During odor stimulation, each oscillation cycle contains both locked and unlocked PN spikes (*36*). Periodic IPSPs, caused in KCs by LHIs whose mean firing is in antiphase with the discharge of the synchronized PNs, antagonize the action of inappropriately timed PN action potentials. When LHI-mediated inhibition is blocked, this normally antagonized excitatory

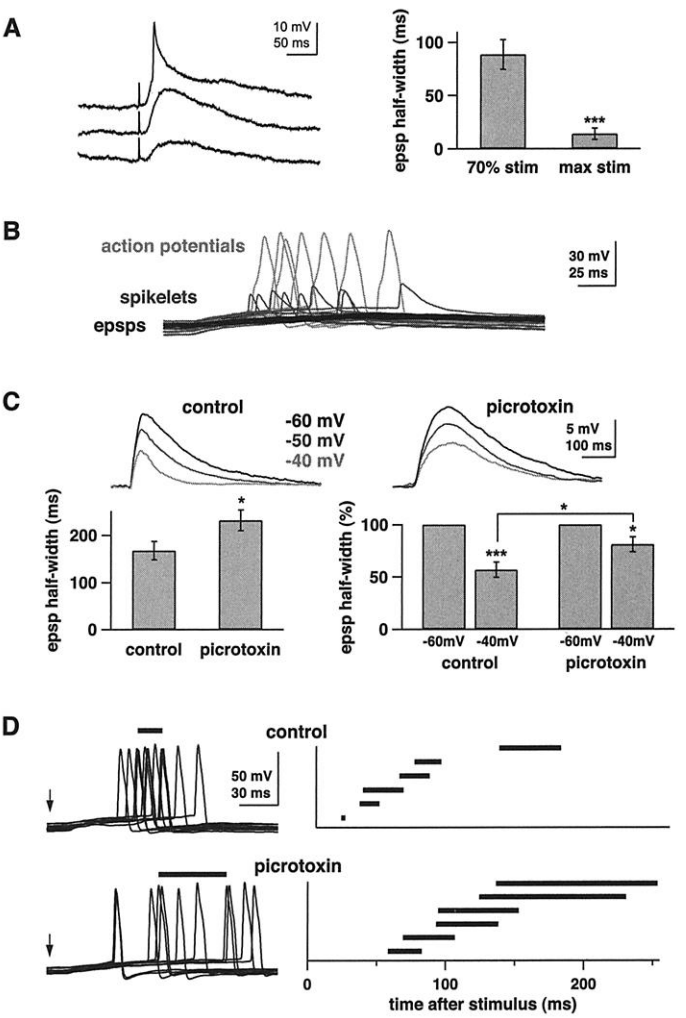

Fig. 5. KC responses to electrical stimulation of PNs. (**A**) PNs were stimulated directly with an electrode placed in the AL and evoked EPSPs were recorded intracellularly from KCs. Three traces show EPSPs recorded at progressively stronger stimulus intensities (bottom to top). Note positive inflexion during rising phase of the top EPSP and sharp repolarization. Bar graph compares EPSP half-width at the maximum stimulus intensity that was still below action potential threshold versus half-width at 70% (±5%) of this maximum intensity. EPSP half-width was significantly different at these two stimulus intensities ($P < 0.001$, paired t test, $n = 11$ KCs). (**B**) Intrinsic active conductance amplifies and sharpens EPSPs near threshold. KC was held near threshold with a constant holding current; PN stimulus amplitude was constant. Successive trials elicited full-blown sodium spikes (light gray), subthreshold EPSPs (black), or intermediate spikelets. Sample traces were collected in PCT; similar spikelets were observed in control conditions (A). (**C**) Synaptic inhibition shortens KC EPSP. At progressively depolarized holding potentials, EPSP half-width significantly decreased (half-width at −40 mV was significantly smaller than half-width at −60 mV; $P < 0.0005$, paired t test, $n = 10$ KCs); all analyzed data were below threshold for spikelet activation. After PCT injection in MB, EPSPs became broader (−60 mV half-width significantly increased in PCT; $P < 0.05$, t test, $n = 9$). EPSP shape was less dependent on postsynaptic voltage (−40 mV half-width as percent of −60 mV half-width significantly increased in PCT; $P < 0.05$, t test, $n = 9$) but was still voltage dependent ($P < 0.05$, t test, $n = 9$). Sample traces are shown from two KCs in the same brain. (**D**) Synaptic inhibition narrows the window in which KCs can fire after PN stimulation. Stimulus intensity was adjusted to elicit an EPSP of 5 to 10 mV (when KC is held at −60 mV), and then holding current was adjusted so that this EPSP elicited a spike on 30% to 60% of trials. Representative traces (left) show those sweeps where spikes were elicited (arrows mark stimulus, bars mark interquartile range of spike times encompassing the difference between the 25th and the 75th percentile). Sample traces are shown from two KCs in the same brain. Group data (right) show the interquartile range for each cell. PCT significantly increased the magnitude of the interquartile ranges ($P < 0.05$, t test, $n = 6$ control KCs, 6 KCs in PCT). (B to D) Whole-cell recordings (*37*).

drive to KCs can now summate over a longer time window: KCs lose much of their specificity. Time-locked feed-forward inhibition thus helps define very short but renewed (once per oscillation cycle) integration windows for each KC, akin to a periodic reset, with critical consequences for KC specificity.

None of the features uncovered so far (oscillatory patterning, feed-forward inhibition, fan-in and fan-out, active properties) are unusual ones (*45–49*). In particular, distributed and partly overlapping projection patterns of mitral cells have been seen in rodent prepiriform cortex (*50*) and local feed-forward inhibitory circuits are common (*45*, *47–49*). Nonlinear intrinsic properties have been seen in some cortical and hippocampal cells among others and hypothesized to underlie coincidence detection (*45*, *46*). We show here that all these properties exist together in the same circuit and that their concerted use in the context of oscillatory activity results in a major transformation of sensory codes.

How could sparsening be useful? Because the MB is a likely site for formation and retrieval of olfactory memories (*30–33*), we must ask why sparse codes might be advantageous there. Although it is clear that extremely sparse codes ("grandmother" schemes) (*51*) may be undesirable because they confer sensitivity to damage and low capacity, representations carried by small subsets of neurons offer many theoretical advantages. First, overlaps between individual representations are less likely than if each representation used a large proportion of the available neurons, limiting interference between memories. This system's memory capacity can still be very high, because the total population size is large and sparseness is not extreme. Second, comparisons between stimulus-evoked patterns and stored memories are simpler if they invoke fewer elements. Similarly, associations (for example, between odors and images) are facilitated. Third, representations become more synthetic or high level. Every KC action potential compresses the signals carried by several PNs that are each potentially more informative about stimulus composition. Sparsened representations thus contain less explicit detail. This conclusion agrees with behavioral and psychophysical observations in humans, rats, and insects that odor perception has a prevalent synthetic quality (*52–54*).

Significance for neural coding. Our results have implications for understanding neural codes. First, single-neuron responses can be exquisitely specific, extremely short (one or two spikes only), and temporally precise (both within and across oscillation cycles). Studies of frontal, motor, and olfactory cortices show rare and very brief firing events, consistent with some of our results (*55–59*). Second, subtle yet highly relevant activity patterns may go undetected with many large-scale brain-activity monitoring techniques: sparse and brief activity is unlikely to be reflected in most macroscopic signals. Yet, as we show here, this may sometimes be all there is. Lastly, to measure the relevant information content of an action potential, one must know how downstream targets interpret it. For example, we showed previously that PN action potentials typically phase-lock to the LFP only during certain (stimulus and PN specific) epochs of a response (*36*). Our results indicate that KCs are more sensitive to phase-locked PN action potentials than to those that occur closer to each LHI-mediated IPSP, whose timing is itself determined by the locked PN population. PN spikes, therefore, are not all equally meaningful to a KC. Even in cases in which firing rates are high, many spikes may be of minimal significance to a target, because they are improperly timed. Here, relevance is determined by interneuronal correlation. Hence, deciphering brain codes requires evaluating these correlations and their consequences on the channeling of information. Conversely, macroscopic oscillations may indicate the existence of neural filters, whose properties will determine the interpretation one should make of a spike train.

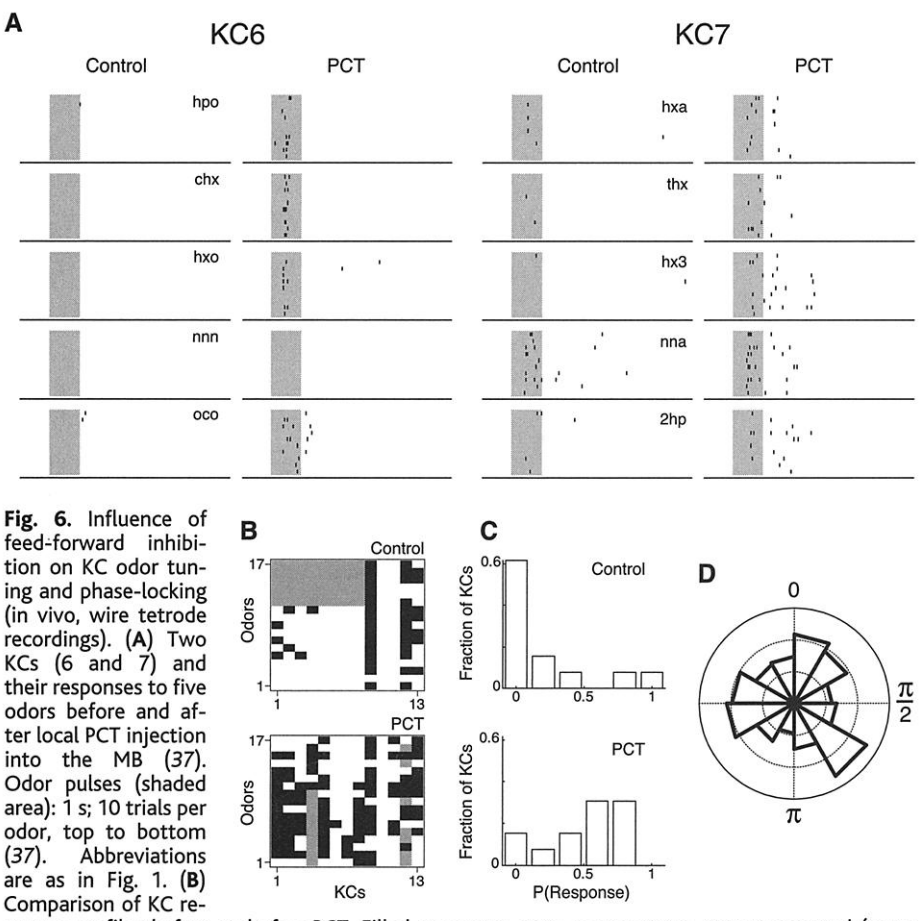

Fig. 6. Influence of feed-forward inhibition on KC odor tuning and phase-locking (in vivo, wire tetrode recordings). (**A**) Two KCs (6 and 7) and their responses to five odors before and after local PCT injection into the MB (*37*). Odor pulses (shaded area): 1 s; 10 trials per odor, top to bottom (*37*). Abbreviations are as in Fig. 1. (**B**) Comparison of KC response profiles before and after PCT. Filled, response; open, no response; gray, not tested (more odors were generally tested after PCT treatment). In a vast majority of KCs, PCT broadened tuning profiles. Odors, 1 to 17: oca, hxa, thx, hx3, oco, unn, nna, 2hp, che, chx, hxo, don, nnn, 3hp, hpo, pnn, min. (**C**) Frequency distribution of response probabilities (across all odors tested) before and after PCT treatment (n = 13 KCs). Note dramatic reduction of proportion of specific KCs (leftmost bin) after PCT treatment. Median response probabilities: 0.09 (control), 0.59 (PCT). (**D**) Phases of KC spikes relative to LFP during odor-evoked responses (0 rad, max; π, min of LFP voltage). Vector strengths: 0.03 (PCT) versus 0.41 (Fig. 4F, control). Gridlines are in intervals of 0.05 (probability per bin).

References and Notes

1. E. Adrian, *J. Physiol.* **100**, 459 (1942).
2. A. Gelperin, D. W. Tank, *Nature* **345**, 437 (1990).
3. C. Gray, *J. Comput. Neurosci.* **1**, 11 (1994).
4. A. Bragin *et al.*, *J. Neurosci.* **15**, 47 (1995).
5. M. Steriade, F. Amzica, D. Contreras, *J. Neurosci.* **16**, 392 (1996).
6. G. Csibra, G. Davis, M. W. Spratling, M. H. Johnson, *Science* **290**, 1582 (2000).
7. C. Gray, P. König, A. Engel, W. Singer, *Nature* **338**, 334 (1989).
8. R. Eckhorn *et al.*, *Biol. Cybern.* **60**, 121 (1988).
9. R. Rodriguez *et al.*, *Nature* **397**, 430 (1999).
10. A. D. Patel, E. Balaban, *Nature* **404**, 80 (2000).
11. P. Fries, J. H. Reynolds, A. E. Rorie, R. Desimone, *Science* **291**, 1560 (2000).
12. A. K. Engel, P. Fries, W. Singer, *Nature Rev. Neurosci.* **2**, 704 (2001).
13. M. N. Shadlen, J. A. Movshon, *Neuron* **2**, 67 (1999).
14. L. Abbott, P. Dayan, *Neural Comput.* **11**, 91 (1999).
15. J. J. Hopfield, *Nature* **376**, 33 (1995).
16. C. von der Malsburg, W. Schneider, *Biol. Cybern.* **54**, 29 (1986).
17. M. Diesmann, M.-O. Gewaltig, A. Aertsen, *Nature* **402**, 529 (1999).
18. M. Abeles, *Isr. J. Med. Sci.* **18**, 83 (1982).

19. P. König, A. K. Engel, W. Singer, *Trends Neurosci.* **19**, 130 (1996).
20. P. J. Clyne *et al.*, *Neuron* **22**, 327 (1999).
21. Q. Gao, B. Yuan, A. Chess, *Nature Neurosci.* **3**, 780 (2000).
22. L B. Vosshall, A. M. Wong, R. Axel, *Cell* **102**, 147 (2000).
23. P. Mombaerts *et al.*, *Cell* **87**, 675 (1996).
24. G. Laurent, M. Naraghi, *J. Neurosci.* **14**, 2993 (1994).
25. Y.-W. Lam, L. Cohen, M. Wachowiak, M. Zochowski, *J. Neurosci.* **19**, 749 (1999).
26. K. MacLeod, A. Bäcker, G. Laurent, *Nature* **395**, 693 (1998).
27. M. Stopfer, S. Bhagavan, B. H. Smith, G. Laurent, *Nature* **390**, 70 (1997).
28. M. Wehr, G. Laurent, *Nature* **384**, 162 (1996).
29. K. MacLeod, G. Laurent, *Science* **274**, 976 (1996).
30. M. Heisenberg, A. Borst, S. Wagner, D. Byers, *J. Neurogenet.* **2**, 1 (1985).
31. J. Dubnau, L. Grady, T. Kitamoto, T. Tully, *Nature* **411**, 476 (2001).
32. S. E. McGuire, P. T. Le, R. L. Davis, *Science* **293**, 1330 (2001).
33. T. Zars, M. Fischer, R. Schulz, M. Heisenberg, *Science* **288**, 672 (2000).
34. F. C. Kenyon, *J. Comp. Neurol.* **6**, 133 (1896).
35. B. Leitch, G. Laurent, *J. Comp. Neurol.* **372**, 487 (1996).
36. G. Laurent, M. Wehr, H. Davidowitz, *J. Neurosci.* **16**, 3837 (1996).
37. Materials and methods are available as supporting material on *Science* Online.
38. Most KC spikes occurred in the beginning of the response: response intensity was 2.33 ± 2.02 spikes over the first 1.4 s; PNs produced 12.84 ± 7.29 spikes on average in that period.
39. Responses were determined here according to method A (*37*). Nearly identical results were obtained if responses were assessed by different criteria adapted to each population (figs. S4 and S5).
40. B. Willmore, D. J. Tolhurst, *Network Comput. Neural Syst.* **12**, 255 (2001).
41. B. S. Hansson, S. Anton, *Annu. Rev. Entomol.* **45**, 203 (2000).
42. Although we have not characterized this spikelet pharmacologically, its shape and all-or-none waveform suggest the involvement of voltage-dependent conductances (possibly Na^+ or Ca^{2+} for depolarization and K^+ for repolarization), consistent with previous patch-clamp studies in vitro (*43*).
43. S. Schafer, H. Rosenboom, R. Menzel, *J. Neurosci.* **14**, 4600 (1994).
44. PCT application to the MB did not affect the LFP oscillations recorded there, for the principal source of these oscillations—synchronized, periodic synaptic input drive from PNs— was excitatory and cholinergic (nicotinic).
45. D. Fricker, R. Miles, *Neuron* **28**, 559 (2000).
46. M. Galarreta, S. Hestrin, *Science* **292**, 2295 (2001).
47. F. Pouille, M. Scanziani, *Science* **293**, 1159 (2001).
48. D. Contreras, A. Destexhe, M. Steriade, *J. Neurophysiol.* **78**, 335 (1997).
49. L. B. Haberly, in *Cerebral Cortex*, E. G. Jones, A. Peters, Eds. (Plenum, New York, 1990), pp. 137–166.
50. Z. Zou, L. F. Horowitz, J.-P. Montmayeur, S. Snapper, L. B. Buck, *Nature* **414**, 173 (2001).
51. H. Barlow, *Ann. N.Y. Acad. Sci.* **156**, 872 (1969).
52. A. Livermore, D. G. Laing, *J. Exp. Psychol. Human Percept. Perform.* **22**, 267 (1996).
53. C. Linster, B. H. Smith, *Physiol. Behav.* **66**, 701 (1999).
54. W. S. Cain, B. C. Potts, *Chem. Senses* **21**, 35 (1996).
55. M. Abeles, H. Bergman, E. Margalit, E. Vaadia, *J. Neurophysiol.* **70**, 1629 (1993).
56. A. Riehle, S. Grün, M. Diesmann, A. Aertsen, *Science* **281**, 34 (1997).
57. P. Duchamp-Viret, B. Palouzier-Paulignan, A. Duchamp, *Neuroscience* **74**, 885 (1996).
58. T. Tanabe, M. Iino, S. F. Takagi, *J. Neurophysiol.* **30**, 1284 (1975).
59. J. W. Nemitz, S. J. Goldberg, *J. Neurophysiol.* **49**, 188 (1983).
60. Supported by the National Institute for Deafness and other Communication Disorders; the National Science Foundation; the McKnight, Alfred P. Sloan, and Keck Foundations (G.L.); a Sloan and Swartz Foundations fellowship (J.P.-O.); a Department of Defense National Defense Science and Engineering graduate fellowship (O.M.); the Elizabeth Ross fellowship (G.C.T.); and a Helen Hay Whitney postdoctoral fellowship (R.I.W.). We thank M. Westman for his intracellular PN data; C. Pouzat for help with spike sorting; S. Farivar for help with the immunocytochemistry; the Laurent Lab; E. Schuman, A. Siapas, and C. Mead for discussions; M. Roukes for help with silicon tetrodes; I. Lubenov and A. Siapas for help with wire tetrodes; M. Walsh for electronics; and the Caltech Biological Imaging Center for their resources and expertise. Multichannel silicon probes were provided by the University of Michigan Center for Neural Communication Technology sponsored by NIH NCRR grant no. P41-RR09754.

Supporting Online Material
www.sciencemag.org/cgi/content/full/297/5580/359/DC1
Materials and Methods
Figs. S1 to S5
Movie S1

4 February 2002; accepted 31 May 2002

Regulation of Cerebral Cortical Size by Control of Cell Cycle Exit in Neural Precursors

Anjen Chenn[1,2]* and Christopher A. Walsh[2]†

Transgenic mice expressing a stabilized β-catenin in neural precursors develop enlarged brains with increased cerebral cortical surface area and folds resembling sulci and gyri of higher mammals. Brains from transgenic animals have enlarged lateral ventricles lined with neuroepithelial precursor cells, reflecting an expansion of the precursor population. Compared with wild-type precursors, a greater proportion of transgenic precursors reenter the cell cycle after mitosis. These results show that β-catenin can function in the decision of precursors to proliferate or differentiate during mammalian neuronal development and suggest that β-catenin can regulate cerebral cortical size by controlling the generation of neural precursor cells.

A massive increase in the size of the cerebral cortex is thought to underlie the growth of intellectual capacity during mammalian evolution. The increased size of larger brains results primarily from a disproportionate expansion of the surface area of the layered sheet of neurons comprising the cerebral cortex (*1–7*), with the appearance of convolutions of the cortical surface (with crests known as gyri and intervening grooves called sulci) providing a means of increasing the total cortical area in a given skull volume. This horizontal expansion of the cerebral cortex is not accompanied by a comparable increase in cortical thickness; in fact, the 1000-fold increase in cortical surface area between human and mouse is only accompanied by an ~twofold increase in cortical thickness (*8*).

The cerebral cortex is organized into columnar functional units (*9*), and the expansion of the cerebral cortex appears to result from increases in the number of radial columns rather than from increases in individual column size (*5*, *10*). These observations have led to the proposal that increases in the number of columns result from a corresponding increased number of progenitor cells (*5*). It has been suggested that minor changes in the relative production of progenitors and neurons could produce dramatic increases in cortical surface area (*5*, *11*).

One protein that might regulate the production of neural precursors is β-catenin, an integral component of adherens junctions (*12*) that interacts with proteins of the T cell factor/lymphoid enhancer binding factor (TCF/LEF) family to transduce Wnt signals (*13*). Wnts (a family of secreted signaling molecules that regulate cell growth and cell fate) (*14*) and TCF/LEF family members (*15*, *16*) are expressed in overlapping patterns in the developing mammalian brain, and numerous studies support the role of Wnt signaling in cell fate regulation during development (*17*). Inactivation of specific Wnts (*18*, *19*), TCF/LEF members (*20*), or β-catenin (*21*) results in specific developmental brain defects, and persistent activation of β-catenin has been implicated in a variety of human cancers (*13*), including some resembling neural precursors such as medulloblastoma (*22*). These findings raise the possibility that β-catenin influences cell number or cell fate decisions in the developing nervous system.

β-catenin is widely expressed in many tissues (*23*). To examine more closely the expression patterns of β-catenin during mammalian

[1]Department of Pathology, Brigham and Women's Hospital, Boston, MA 02115, USA. [2]Division of Neurogenetics, Department of Neurology, Beth Israel Deaconess Medical Center, Boston, MA 02115, USA.

*Present address: Department of Pathology, Northwestern University School of Medicine, 303 East Chicago Avenue, Chicago, IL 60611–3008, USA.
†To whom correspondence should be addressed. E-mail: cwalsh@caregroup.harvard.edu